Fast and accurate calibration-based thermal / colour sensors registration

by L. St-Laurent*,**, D. Prévost** and X. Maldague*

*ECE Dept., Université Laval, Québec (Quebec), Canada G1V 0A6, louis.st-laurent@ino.ca
**INO, Québec (Quebec), Canada G1P 4S4, donald.prevost@ino.ca

Abstract

Combination of thermal and electro-optical sensors is useful in numerous applications related to inspection and monitoring. A few manufacturers already offer hybrid thermal / colour cameras. However, those off-the-shelf products generally provide independent images from both sensors whereas an accurate pixel-by-pixel registration would be greatly beneficial for most applications. This paper presents a calibration-based approach allowing the acquisition of co-registered thermal / visible videos with a simple side-by-side camera configuration. The proposed method has the interesting capabilities of accurately registering both fields of view by a single image mapping More specifically, this mapping converts distorted image coordinates from thermal image to corresponding distorted image coordinates of colour image. Once computed, the projection matrix can be optimized for a specific object distance. An original calibration rig optimized for the thermal spectrum is also presented.

1. Introduction

Registration of thermal and electro-optical sensors is a challenging task due to the dissimilarity of feature appearance in both spectral bands. Approaches based on matching of corresponding features observed / detected in the scene are generally inaccurate, especially if no attention has been devoted to optical axes alignment. A much more efficient technique is to take into account physical properties of the acquisition platform (relative position, relative orientation, lens aberrations, etc.) in order to deduce corresponding pixels coordinates from both sensors. This is calibration-based registration.

Two hardware configurations can be used for accurate pixel-by-pixel registration: parallel / convergent or superposed optical axes. Superposition of optical axes can be achieved with the use of a beamsplitter [4][5] or catadioptric optics [1]. Such configurations provide the advantage that image registration is valid for a wide depth of field, which can be a critical requirement for some applications. However, these designs are more expensive and their assembly is more complex because of additional optic components. Another drawback of existing superposed optical axes configurations is their limited field of view (around 20 degrees for catadioptric designs [1] and 45 degrees with beamsplitter configurations)

Parallel / convergent optical axes configuration is much simpler since it only requires placing cameras side-by-side and accurately aligning optical axes. This is the configuration addressed in this paper. The main limitation of side-by-side configuration is that image registration is valid only for a specific target distance (D_{target}). Mathematically, registration errors δ_x (expressed in pixels) for side-by-side configuration is determined by:

$$\delta_x = \frac{f \cdot d_c}{l_{pix}} \cdot \left(\frac{1}{D_{target}} - \frac{1}{D_{optimal}} \right) \tag{1}$$

where f is focal length, l_{pix} is pixel sixe and d_c is the baseline (the lateral distance between sensors principal points). $D_{optimal}$ is the target distance where perfect alignment is obtained (no registration error). If optical axes are parallel, $D_{optimal} = \infty$ since only targets located very far from the acquisition platform will be aligned with precision. Any scene element located closer ($D_{target} < \infty$) will suffer registration error. Depending on application and scene, perfect registration may be required for a specific target distance $D_{optimal}$. It is possible to achieve this by translating one image along baseline orientation or by slightly rotating one camera such that optical axes will converge at exactly this distance.

In this work, we demonstrate that although side-by-side configuration provides perfect image registration only for a specific target distance, a conscientious sensor alignment technique can make registration errors negligible for many applications. Apart from introduction (section 1) and conclusion (section 5), this paper is divided in three sections. In section 2, we present the thermal calibration rig designed and built during this project. Section 3 is the main contribution as it describes in details the four calibration steps proposed. The purpose of this approach is to enable the user of the acquisition platform to accurately register both fields of view by a single image mapping and easily optimize the alignment for a specific

target distance. Section 4 includes registration accuracy analysis and examples of co-registered LWIR-colour images obtained with the acquisition platform developed at INO.

2. Thermal calibration rig

Internal calibration of electro-optical cameras is a common task in the vision community and off-the-shelf calibration rigs are available. However, internal calibration of thermal cameras is a new challenge. For this purpose, we developed a geometric calibration rig (right of figure 1) designed to generate highly contrasted features in thermal spectral ranges (MWIR and LWIR). Its main components are a silicon rubber heater that acts as a source of thermal radiations and a plastic mask with a grid of holes. The concept is that when the rig is powered, the rubber heater warms up while the mask remains at room temperature, creating thermal contrast. Mask holes can then be accurately extracted in images.

We placed side by side two 1 x 2 ft silicon rubber heater mats and perforated the mask with 49 evenly spaced 1.25 inch diameter holes to form a calibration rig of suitable size (2 x 2 ft) for our sensor registration needs. A smaller size would offer limited performances at steps 2 and 3 of the proposed calibration methodology (section 3). Moreover, most thermal cameras with fixed lens are assembled to generate sharp images of objects located far from the camera (more than one meter). Too small a calibration rig would require it to be placed closer to the camera for internal calibration (step 1 of section 3), thus leading to blurred image features.

Since the silicon rubber heater is very thin, it was glued to a 2 inch thick polystyrene panel for rigidity as well as thermal insulation. The plastic mask is fixed to silicon rubber heater sheets via 1.5 inch long low conductivity plastic cylinders. The rear surface of the plastic mask was also covered with aluminum tape to minimize heat transfer by radiation. To avoid introducing bias on automatic circular holes localization, the border of every hole was chamfered, bringing the mask thickness to zero at holes borders. This way, holes appear perfectly circular or oval even if the calibration rig is not held perpendicular to the camera.

Finally, special attention must be devoted to paint selection to maximize holes emissivity and minimize mask reflectivity. As shown on figure 1, a high emissivity black paint was applied on the silicon rubber heater mats and a high emissivity white paint on the mask. A plastic mask having a rough surface (by opposition to polished finish) is also required to minimize thermal reflection from ambient sources like room lights. The white / black contrast is required for steps 2 and 3 (section 3) where holes must be visible in both thermal and electro-optical images. In fact, the designed calibration rig could also be used for internal calibration (step 1) of electro-optical sensor if no checkerboard or high performance calibration rig (left of figure 1) is available.

3. Proposed calibration methodology

Pixel-to-pixel alignment can't be obtained by simply fixing two cameras side-by-side. Because of distinct characteristics, like resolution, focal length, pixels size and lens distortions, a cascade of operations must be applied to get accurate registration. The purpose of our calibration-based approach is to concatenate all these operations in a single transformation. We propose a rigorous 4-step calibration procedure to achieve this:

1- Determination of internal parameters for both thermal and electro-optical sensors.
2- Optical axes alignment.
3- Determination of tilt angle and field of view ratio between sensors.
4- Generation of look-up tables (LUT)

Steps 1 to 3 are performed once and all parameters are stored in a file. Step 4 can thus be performed every time a new optimal target distance is specified by the user of the acquisition platform. Every phase is detailed in the following sub-sections.

3.1. Determination of internal parameters

A total of 15 intrinsic parameters are estimated for both sensors of the thermal / colour acquisition platform during this first calibration step. They are listed in table 1. Our camera model is based on the well known « Camera Calibration Toolbox for MATLAB » [6] developed by Dr Jean-Yves Bouguet, from *California Institute of Technology*. This is an open source MATLAB implementation of the model proposed by Heikkila and Silven [3], which is broadly accepted in the computer vision community.

Following the convention of [6], the relation between distorted normalized coordinate (u_d, v_d) and rectified normalized coordinate (u_n, v_n) is given by equation 2. The same model, but with different distortion coefficients, can be used

to get the rectified normalized coordinate from the distorted normalized coordinate (equation 3). The relation between normalized coordinate (*u, v*) (without unit) and image coordinate (*x, y*) expressed in pixels is given at equation 4.

***Table 1** : Estimated internal parameters.*

Description	Notation
Focal length [in pixels]	fc_x , fc_y
Principal point location [in pixels]	x_0 , y_0
Tilt angle between sensor axes x and y	α
Radial (k_i) and tangential (p_i) distortion coefficients	k_1 , k_2, , k_3 p_1 , p_2
Inverse radial (k_inv_i) and tangential (p_inv_i) distortion coefficients	K_inv_1 , k_inv_2 , k_inv_3 p_inv_1 , p_inv_2

$$\begin{bmatrix} u_d \\ v_d \end{bmatrix} = \begin{bmatrix} u_n \cdot \left(1 + k_1 \cdot r^2 + k_2 \cdot r^4 + k_3 \cdot r^6\right) + 2 \cdot p_1 \cdot u_n \cdot v_n + p_2 \cdot \left(r^2 + 2 \cdot u_n^2\right) \\ v_n \cdot \left(1 + k_1 \cdot r^2 + k_2 \cdot r^4 + k_3 \cdot r^6\right) + p_1 \cdot \left(r^2 + 2 \cdot v_n^2\right) + 2 \cdot p_2 \cdot u_n \cdot v_n \end{bmatrix} \quad \text{where} \quad r^2 = u_n^2 + v_n^2 \tag{2}$$

$$\begin{bmatrix} u_n \\ v_n \end{bmatrix} = \begin{bmatrix} u_d \cdot \left(1 + k\_inv_1 \cdot r^2 + k\_inv_2 \cdot r^4 + k\_inv_3 \cdot r^6\right) + 2 \cdot p\_inv_1 \cdot u_d \cdot v_d + p\_inv_2 \cdot \left(r^2 + 2 \cdot u_d^2\right) \\ v_d \cdot \left(1 + k\_inv_1 \cdot r^2 + k\_inv_2 \cdot r^4 + k\_inv_3 \cdot r^6\right) + p\_inv_1 \cdot \left(r^2 + 2 \cdot v_d^2\right) + 2 \cdot p\_inv_2 \cdot u_d \cdot v_d \end{bmatrix} \quad \text{where} \quad r^2 = u_d^2 + v_d^2 \tag{3}$$

$$\begin{bmatrix} x \\ y \\ 1 \end{bmatrix} = \begin{bmatrix} fc_x & \alpha \cdot fc_x & x_0 \\ 0 & fc_y & y_0 \\ 0 & 0 & 1 \end{bmatrix} \cdot \begin{bmatrix} u \\ v \\ 1 \end{bmatrix} \tag{4}$$

To estimate the 15 parameters of table 1 for each sensor, a calibration rig must be placed in front of the camera and its *N* features (usually circles or corners) must be localized in the image. Based on these image coordinates and on a priori knowledge of real relative position of calibration rig features, non-linear optimization can be performed to estimate coefficients of equations 2 and 4. Obviously, the amplitude of estimation errors is mainly dependant on position accuracy of segmented features. It is why suitable calibration rigs must be used for thermal and electro-optical spectral bands to achieve accurate internal calibration. Those that we used are illustrated in figure 1. The electro-optical calibration rig is 3-D and has been designed at INO for applications requiring high accuracy. An off-the-shelf 2-D checkerboard calibration rig could also be used, which would certainly be sufficiently accurate for our sensor registration task. The benefit of a 3-D rig is that it allows performing internal calibration with a single camera snap-shot comparatively to a few images with a 2-D rig. As described in section 2, the thermal calibration rig has been designed and built at INO especially for this work. Both rigs have circular features since it has been demonstrated that automatic image extraction of circular features is slightly more accurate than localization of corners of checkerboard pattern [2].

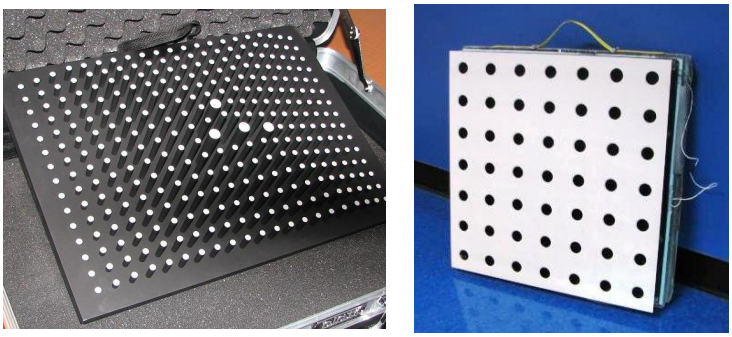

***Fig. 1.** Electro-optical (left) and thermal (right) calibration rigs developed at INO.*

We estimate parameters of equations 2 and 4 (first 10 of table 1) via non-linear optimization method embedded in [6]. With these coefficients for both sensors, it is possible to rectify (correction of radial and tangential distortions) thermal and colour images independently. Examples of rectified images are presented at figure 2. The significant pincushion shape of both reconstructed images (meaning that both images suffer from barrel distortion) confirms the necessity to consider these aberrations in the sensor registration process. It also invalidates the common hypothesis that germanium lens aberrations can be considered as negligible, especially for lens with wide field of view.

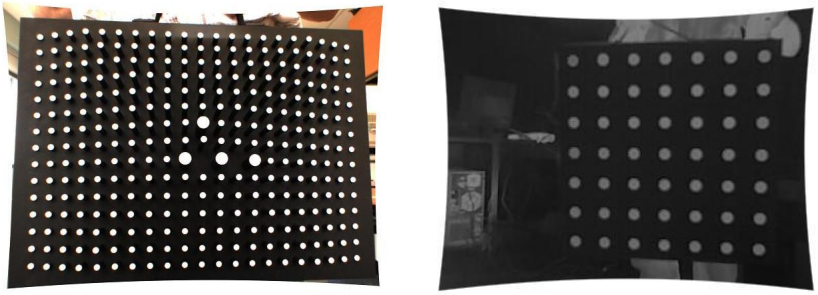

Fig. 2. *Example of rectified electro-optical (left) and thermal (right) images of calibration rigs developed at INO.*

Since our objective is to convert distorted image coordinates from thermal image to corresponding distorted image coordinates of colour image, we also need to estimate inverse transform coefficients of equation 3 (last 5 of table 1). Contrarily to the other parameters, these can be determined directly by solving a linear equations system. As proposed in [3], N pairs of corresponding points (u_n, v_n) and (u_d, v_d) can be generated via equation 2 and already know coefficients. In our case, a grid of 60 x 45 points uniformly distributed on the image surface is used, generating a system of 5400 equations as represented by equation 5. Coefficients of the $\boldsymbol{X}$ vector can then be obtained by singular value decomposition (SVD).

$$\underset{\mathbf{A}}{\begin{bmatrix} r^2u_{d,1} & r^4u_{d,1} & r^6u_{d,1} & 2u_{d,1}v_{d,1} & r^2+2u_{d,1}^2 & u_{d,1}-u_{n,1} \\ r^2v_{d,1} & r^4v_{d,1} & r^6v_{d,1} & r^2+2v_{d,1}^2 & 2u_{d,1}v_{d,1} & v_{d,1}-v_{n,1} \\ \cdots & \cdots & \cdots & \cdots & \cdots & \cdots \\ r^2u_{d,N} & r^4u_{d,N} & r^6u_{d,N} & 2u_{d,N}v_{d,N} & r^2+2u_{d,N}^2 & u_{d,N}-u_{n,N} \\ r^2v_{d,N} & r^4v_{d,N} & r^6v_{d,N} & r^2+2v_{d,N}^2 & 2u_{d,N}v_{d,N} & v_{d,N}-v_{n,N} \end{bmatrix}} \cdot \underset{\mathbf{X}}{\begin{bmatrix} k\_inv_1 \\ k\_inv_2 \\ k\_inv_3 \\ p\_inv_1 \\ p\_inv_2 \\ 1 \end{bmatrix}} = \underset{\mathbf{0}}{\begin{bmatrix} 0 \\ 0 \\ 0 \\ 0 \\ 0 \\ 0 \end{bmatrix}} \tag{5}$$

3.2. Optical axes alignment

This step is the only one involving mechanical alignment manipulations. As mentioned in introduction, perfect registration at a specific target distance $D_{optimal}$ may be achieved by slightly rotating one camera such that optical axes will converge at exactly this distance. More specifically, cameras should be oriented such that the same feature localized at the desired distance $D_{optimal}$ in the scene is observed at the principal point of each sensor (coordinates x_0 and y_0 estimated previously for each camera and listed in table 1). Obviously, the scene feature selected for this task must present good contrast in both spectral bands. Thanks to its black / white contrasting paint, our thermal calibration rig is the ideal tool.

For large required $D_{optimal}$, it can be difficult to really place the rig at this distance. To be able to perform this calibration step in indoor lab, one needs to place the rig at a shorter distance from the acquisition platform and simulate the real distance by translating one image along the baseline orientation. Here is a numerical example. Let's assume that $D_{optimal}$ for some application is 50 m and that the calibration rig is placed at 10 m (D_{target}) from the camera. Equation 1 indicates that a registration error of -1.47 thermal pixel should be observed:

$$\delta_x = \frac{f \cdot d_c}{l_{pix}} \cdot \left(\frac{1}{D_{target}} - \frac{1}{D_{optimal}} \right) = \frac{14.25 \cdot 49}{0,038} \cdot \left(\frac{1}{50000} - \frac{1}{10000} \right) \cong -1,47 \text{ pixel} \tag{6}$$

In our acquisition platform, the thermal camera is fixed on the left of the colour camera (seen from behind). This means that we need to translate the thermal image to the left to simulate a calibration rig distance of 50 m. This offset should be applied only while the user manually adjusts camera orientations. Once completed, the translation is eliminated.

3.3. Determination of tilt angle and field of view ratio

Once internal parameters are known and optical axes are aligned, the three required external parameters may be estimated. They are listed in Table 2. The relative tilt angle (θ) is required to compensate imperfect alignment of *x* and *y* axes of both rectified images, while FOV ratios S_x and S_y are used to scale the thermal FOV to the electro-optical FOV.

***Table 2** : Estimated external parameters.*

Description	Notation
Tilt angle	θ
Fields of view ratio (FOV_{EO} / FOV_{IR})	S_x, S_y

The proposed approach to estimate the tilt angle is to extract corresponding features in electro-optical and thermal images and to compare their angular position relatively to their respective principal point (x_0, y_0):

$$\theta_{p,IR} = \arctan\left(\frac{-\left(y_{IR} - y_{0,IR}\right)}{\left(x_{IR} - x_{0,IR}\right)}\right) + f\left(p\right) \qquad \theta_{p,EO} = \arctan\left(\frac{-\left(y_{EO} - y_{0,EO}\right)}{\left(x_{EO} - x_{0,EO}\right)}\right) + f\left(p\right) \tag{7}$$

f(p) is an angular correction based on the quadrant in which is located the feature *p* (top right : *f(p)* = 0, top left and bottom left : *f(p)* = π, bottom right : *f(p)* = 2π). The purpose of this correction is to express angular positions between 0 and 2π counter clockwise starting at *x* axis. Note that rectified features coordinates must be used in equation 7.

Once again, our thermal calibration rig can be used to generate contrasting features in both spectral ranges. Obviously, the higher the number of corresponding features extracted, the more accurate the tilt angle estimation will be. Moreover, features must be spread within the whole FOV. To generate them, one needs to slowly sweep the FOV with the calibration rig and grab this video sequence. The 49 circular holes may then be extracted and matched offline for every frame, either automatically or semi-automatically.

As for the optical axis alignment step, the target distance of extracted features must be considered. Ideally, features should be located at $D_{optimal}$ to remove registration error δ_x from the tilt angle estimation. For practical reasons, and also because more accurate sub-pixel feature extraction is obtained on the center of an ellipse than on a point [2], it is more suitable to sweep the FOV with the calibration rig at a closer target distance. Thus, position of features extracted in the thermal image must be corrected by shifting its coordinate similarly to equation 5.

The tilt angle θ of the thermal image relatively to the electro-optical image can be estimated by the median of the differences between angular positions of corresponding features *p* (equation 8). We recommend using median instead of mean because features located close to the principal point are affected by large uncertainty that can significantly affect the mean value.

$$\theta = mediane\left\{\theta_{p,RGB} - \theta_{p,T}\right\}_{p=1:P} \tag{8}$$

Once tilt angle is determined, ratios S_x and S_y can be accurately estimated. Similarly, FOV ratios can be estimated by extracting corresponding features in electro-optical and thermal images and by comparing their distance relatively to their respective principal point (x_0, y_0):

$$\begin{aligned} dx_{p,IR} &= \cos\left(\theta\right)\cdot\left(x_{p,IR} - x_{0,IR}\right) - \sin\left(\theta\right)\cdot\left(y_{p,IR} - y_{0,IR}\right) \\ dy_{p,IR} &= \sin\left(\theta\right)\cdot\left(x_{p,IR} - x_{0,IR}\right) + \cos\left(\theta\right)\cdot\left(y_{p,IR} - y_{0,IR}\right) \end{aligned} \qquad \begin{aligned} dx_{p,EO} &= x_{p,EO} - x_{0,EO} \\ dy_{p,EO} &= y_{p,EO} - y_{0,EO} \end{aligned} \tag{9}$$

The same corresponding features than those used for tilt angle estimation can be used, but coordinates of thermal features must be corrected for tilt angle as written in equation 8. Once again, it is the median of distance ratios that is the most suitable metric:

$$S_x = mediane\left\{\frac{dx_{p,EO}}{dx_{p,IR}}\right\}_{p=1:P} \qquad S_y = mediane\left\{\frac{dy_{p,EO}}{dy_{p,IR}}\right\}_{p=1:P} \tag{10}$$

3.4. Generation of look-up tables

The last step consists in determining, for every electro-optical pixel, the exact sub-pixel coordinate of the corresponding thermal point. This can be performed by the succession of transformations listed in table 3. The order of operation must be respected. Subscripts *d* and *n* refer to distorted and rectified normalized coordinates respectively. Also notice that a subtraction or an addition must be performed in transformation #4 depending on relative position of cameras. In our acquisition platform, the thermal camera is fixed on the left of the colour camera (as seen from behind), so a subtraction is required. If cameras were installed one on top of the other, the compensation should instead be applied on the *y* coordinate.

***Table 3** : Succession of transformations.*

#	Description	Mathematic formulation
1	Conversion from electro-optical image coordinate (x_d, y_d) into normalized coordinate (u_d, v_d)	$\begin{bmatrix} u_d \\ v_d \\ 1 \end{bmatrix} = \begin{bmatrix} fc_{x,EO} & \alpha_{EO} \cdot fc_{x,EO} & x_{0,EO} \\ 0 & fc_{y,EO} & y_{0,EO} \\ 0 & 0 & 1 \end{bmatrix}^{-1} \cdot \begin{bmatrix} x_d \\ y_d \\ 1 \end{bmatrix}$
2	Rectification of normalized electro-optical coordinate	Equation 3
3	Conversion of rectified normalized coordinate (u_n, v_n) into rectified pixel coordinate (x_n, y_n) centered on principal point.	$\begin{bmatrix} x_n \\ y_n \\ 1 \end{bmatrix} = \begin{bmatrix} fc_{x,EO} & \alpha_{EO} \cdot fc_{x,EO} & 0 \\ 0 & fc_{y,EO} & 0 \\ 0 & 0 & 1 \end{bmatrix} \cdot \begin{bmatrix} u_n \\ v_n \\ 1 \end{bmatrix}$
4	Shift for registration optimized at a specific target distance D_{target}	$\hat{x}_n = x_n - \left[\frac{f_{EO} \cdot d_c}{l_{pix,EO}} \cdot \left(\frac{1}{D_{optimal}} - \frac{1}{D_{target}}\right)\right]$
5	Compensation for FOV difference	$x_{n,IR} = \hat{x}_{n,EO} / S_x$ $y_{n,IR} = y_{n,EO} / S_y$
6	Compensation for tilt angle	$x'_n = x_{n,IR} \cdot \cos(\theta) - y_{n,IR} \cdot \sin(\theta)$ $y'_n = x_{n,IR} \cdot \sin(\theta) + y_{n,IR} \cdot \cos(\theta)$
7	Conversion of image coordinate centered on principal point (x'_n, y'_n) into normalized coordinate (u_n, v_n)	$\begin{bmatrix} u_n \\ v_n \\ 1 \end{bmatrix} = \begin{bmatrix} fc_{x,IR} & \alpha_{IR} \cdot fc_{x,IR} & x_{0,IR} \\ 0 & fc_{y,IR} & y_{0,IR} \\ 0 & 0 & 1 \end{bmatrix}^{-1} \cdot \begin{bmatrix} x'_n + x_{0,IR} \\ y'_n + y_{0,IR} \\ 1 \end{bmatrix}$
8	Inverse rectification of normalized thermal coordinate	Equation 2
9	Conversion from normalized coordinate (u_d, v_d) into thermal coordinate (x_d, y_d)	$\begin{bmatrix} x_d \\ y_d \\ 1 \end{bmatrix} = \begin{bmatrix} fc_{x,IR} & \alpha_{IR} \cdot fc_{x,IR} & x_{0,IR} \\ 0 & fc_{y,IR} & y_{0,IR} \\ 0 & 0 & 1 \end{bmatrix} \cdot \begin{bmatrix} u_d \\ v_d \\ 1 \end{bmatrix}$

The only remaining task is to determine image coordinates and multiplicative coefficients of the four neighbours required to performed bilinear interpolation of thermal intensity values. It is those four indexes and four coefficients for every electro-optical pixel that are stored in LUTs and used for real-time image registration.

4. Registration accuracy

The proposed calibration-based registration method has been used with hybrid LWIR / colour acquisition platforms developed at INO. As illustrated on figure 3, these thermal / electro-optical cameras are currently used at INO in various applications related to video monitoring in outdoor environment. Their specifications are listed in table 4. Note that the 5.02 mm focal length of the colour camera is calculated from internal parameters since a vari-focal lens is used. Before the calibration, the focal length of the colour camera is manually adjusted in such a way that the thermal FOV is enclosed in electro-optical FOV.

Fig. 3. *LWIR / colour acquisition platform developed at INO.*

Table 4 *: Specifications of hybrid LWIR / colour acquisition platforms developed at INO.*

	Colour camera	Thermal camera
Resolution [pixels]	1024 x 768	320 x 240
Pixel size (l_{pix}) [µm]	4.648	38
Focal length (f) [mm]	5.02	14.25
Baseline (d_c) [mm]	49	

Curves of figure 3 give the registration errors obtained with such acquisition platform specifications. The dotted line is for $D_{optimal} = \infty$ while the solid line is for $D_{optimal}$ = 50 m (no registration error for features located at 50 m). Registration errors are expressed in pixels of the generated RGBT image, which has a resolution of 448 x 326 pixels. This output resolution results from the decimation of the electro-optical image by a factor 2 and from the cropping of rows and columns not completely covered by fields of view of both sensors. The electro-optical image is decimated to avoid exaggerated extrapolation of the smaller thermal image.

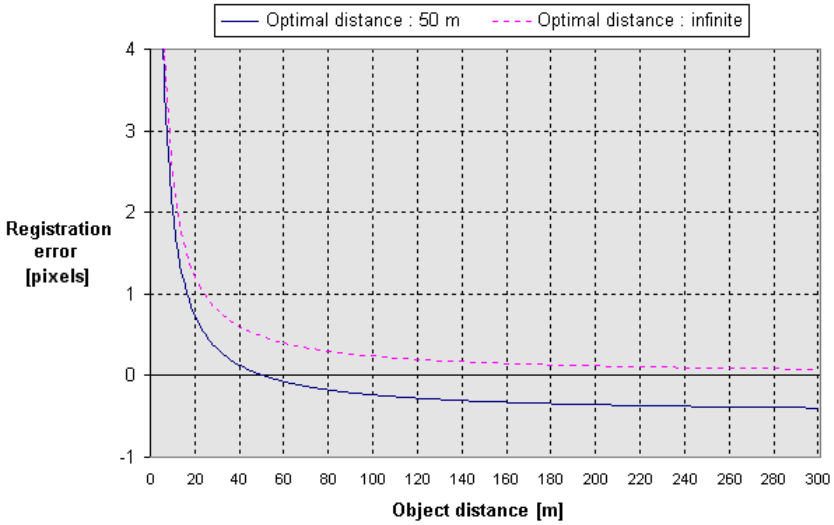

Fig. 3. *Registration errors as a function of target distance.*

We can visualize on figure 3 that when $D_{optimal}$ = 50 m, a feature located at 25 m from the camera will suffer a registration error of around 0.5 pixel:

$$\delta_x = \frac{f \cdot d_c}{l_{pix}} \cdot \left(\frac{1}{D_{\text{target}}} - \frac{1}{D_{\text{optimal}}} \right) = \frac{5.02 \cdot 49}{(2 \cdot 0.004648)} \cdot \left(\frac{1}{25000} - \frac{1}{50000} \right) = 0.529 \text{ pixel} \qquad (11)$$

This means that if the acceptable registration error for some application is ±0.5 pixel, the valid target distance with this configuration is 25 m to infinite. This requirement may then be achieved by a consequent positioning of the acquisition platform. For example, fixing the camera on a 25 m post or on a building located 25 m from the closest point of the target area would ensure that requirement on registration error is respected. Note that in most video monitoring applications with large depth of field, a larger registration error may be acceptable on close targets because their larger image size make them less sensitive to registration errors.

Mathematical formulation of registration error (equation 1) reveals that, apart from target and optimal distances, registration error amplitude depends on baseline (d_c) and pixel size (l_{pix}). Interestingly, it is also proportional to focal length (f). This indicates that setups with large field of view (short focal length) will be less affected by registration errors for the same target distance.

Registration accuracy provided by the proposed calibration-based method may be demonstrated by replacing the red channel by the thermal image. Such examples are presented in figure 4 even though monochrome printing only renders a limited visualization quality.

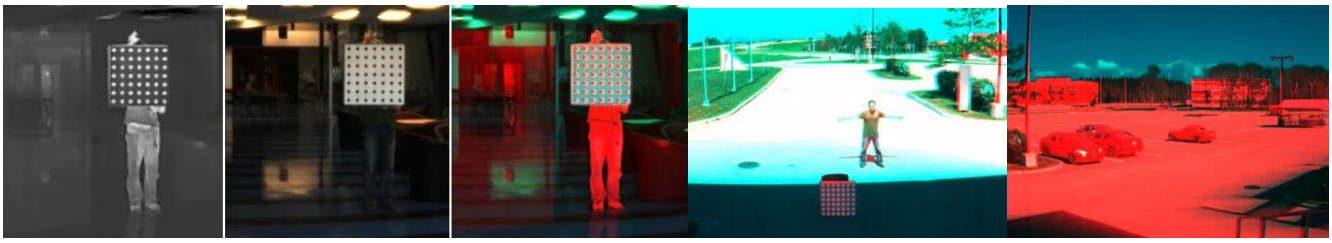

Fig. 4. *Visualization of registration accuracy.*

5. Conclusion

A calibration-based approach allowing the acquisition of co-registered thermal / visible videos with a simple side-by-side camera configuration is presented. The proposed four steps calibration method has the interesting capabilities of accurately registering both fields of view by a single image mapping, which is perfectly suited for real-time processing. Once computed, the projection matrix can be easily modified by the user to optimize the registration accuracy for a specific target distance. This is an attractive characteristic for acquisition platforms devoted to various applications.

Side-by-side configuration offers satisfying registration accuracy for applications looking at a very small depth of field (all features of interest are at same object distance). We demonstrated in this work that the registration accuracy achieved with the proposed calibration-based approach would also fulfill requirements of most wide fields of view video monitoring applications.

Another contribution is the design of a calibration rig optimized for the thermal spectrum. Thanks to its silicon rubber heater mats that act as a source of thermal radiations and its contrasting black and white appearance, the rig provides circular features that can be easily and accurately extracted in both electro-optical and thermal spectrums. The calibration rig is thus not only useful for internal calibration of thermal cameras, it is also perfectly suited for thermal / electro-optical sensors registration.

REFERENCES

[1] Bergeron A. et al., “Novel lightweight uncooled thermal weapon sight”, SPIE vol.5406, *Infrared Technology and Applications XXX,* p.402-411, 2004.

[2] Heikkilä, J., “Geometric camera calibration using circular control points", *IEEE Trans. on Pattern Analysis and Machine Intelligence*, vol.22, no.10, 2000, pp.1066-1077.

[3] Heikkila J. and Silven O., “A four-step camera calibration procedure with implicit image correction”, *IEEE Conf. on Computer vision and Pattern Recognition*, San Juan (Porto Rico), p.1106-1112, 1997.

[4] St-Laurent L., Prévost D. and Maldague X., “Thermal imaging for enhanced foreground-background segmentation”, *Int. Conf. on Quantitative InfraRed Thermography*, Padova (Italy), 10 p., 2006.

[5] http://www.freepatentsonline.com/6781127.pdf, patent number US6781127 belonging to Equinox Corporation, New York, NY, USA, inventors L.B. Wolff and M. Hutt, 2004.

[6] http://www.vision.caltech.edu/bouguetj/calib_doc/index.html, Web site of “*Camera Calibration Toolbox for Matlab*” developed by Dr Jean-Yves Bouguet, *California Institute of Technology*, Pasadena, CA, USA.